FIRST RESULTS OF THE OROMA EXPERIMENT IN THE LISTER TIEF OF THE GERMAN BIGHT IN THE NORTH SEA

Ingo Hennings[1], Dagmar Herbers[1], Katharina Prinz[2] and Friedwart Ziemer[2]

1. Leibniz-Institut für Meereswissenschaften IFM-GEOMAR an der Christian-Albrechts-Universität zu Kiel, 24148 Kiel, Germany; ihennings(at)ifm-geomar.de
2. GKSS-Forschungszentrum Geesthacht GmbH, Institut für Küstenforschung, 21502 Geesthacht, Germany; friedwart.ziemer(at)gkss.de

ABSTRACT

The objective of the project entitled "Operational Radar and Optical Mapping in monitoring hydrodynamic, morphodynamic and environmental parameters for coastal management (OROMA)" within the Fifth Framework Programme of the European Commission (EC) is to improve the effectiveness of monitoring technologies in coastal waters. The Research Vessel (R.V.) *Ludwig Prandtl* of the GKSS research centre was equipped with special sensors and instruments to measure the position of the ship, the water depth, the salinity, the water temperature, the current speed and direction, the modulation characteristics of short-wave energies, and relevant air-sea interaction parameters due to the presence of submarine sand waves. The first experiment of the OROMA project on 5-16 August 2002 took place in the Lister Tief, a tidal inlet of the German Bight in the North Sea. The seabed morphology of the Lister Tief reveals a complex configuration of different bedforms which is four-dimensional in space and time. A significant upward orientated component u_{vert} of the three-dimensional current velocity field was observed. Marked vertically so-called waterspouts of u_{vert} above the crests of sand waves have been measured by the Acoustic Doppler Current Profiler (ADCP) as straight lines. They cause water upwelling with turbulence patterns at the water surface affecting the Normalized Radar Cross Section (NRCS) modulation. A first impression of expected NRCS modulation signatures of sea bottom topography detected by the GKSS shipborne X-band radar are presented as an uncalibrated composite of five single sea clutter images acquired in the Lister Tief on 22 November 1990.

Keywords: North Sea; marine sand waves; Acoustic Doppler Current Profiler (ADCP); Normalized Radar Cross Section (NRCS) modulation

INTRODUCTION

De Loor and co-workers in The Netherlands gave a first description of radar signatures of submarine sand waves in coastal waters. They had noticed such surface manifestations in airborne radar imagery acquired in 1969 at the Dutch coast of the southern North Sea (1). SEASAT, the first satellite specifically designed to study the oceans was launched in 1978. One of the instruments aboard, the Synthetic Aperture Radar (SAR), gathered data of unexpected sea surface signatures that clearly showed the ocean floor. At that time the SEASAT L-band SAR recorded spectacular images of bottom topography in shallow seas like the Great Bahama Bank Southern Edge Tongue of the Ocean, the southern North Sea, the English Channel, the Thames Estuary, the Irish Sea, the Bristol Channel, and the Nantucket Shoals (2,3). Theoretical models of the radar imaging mechanism of sea bottom topography have been described by (2,3,4,5,6,7) and two of these models have been discussed by (8). Nowadays, signatures of Normalized Radar Cross Section (NRCS) modulations at the ocean surface due to sea bottom topography are visible on a variety of radar images derived by shore- and ship-based radar as well as by Real Aperture Radar (RAR) and Synthetic Aperture Radar (SAR) on board air- and spaceborne platforms (7,9).

Many advances in understanding the radar imaging mechanism of the seabed topography have been realized already within the field experiment of the Coastal Sediment Transport Assessment using SAR imagery (C-STAR) project of the MAST-III program of the EC (10). Basic data of rele-

vant hydrodynamic processes have been collected in the southern North Sea using an airborne SAR and a special buoy system, which drifted across large sand waves. SAR images and *in situ* wave energy density measurements were acquired quasi simultaneously. This offered, for the first time, the possibility to compare P-band NRCS modulations and corresponding spectral wave energy density variations to test if the first order Bragg scattering mechanism is applicable: both profiles compared fairly well, taking into account the lower spatial resolution of the wave energy density measurements.

The classical way of receiving valuable information of submarine bedforms is the extensive use and analysis of side scan sonar records and single- as well as multibeam echo sounding data. Recently, airborne lidar (Light Detection and Ranging) bathymetry (ALB) techniques have become more and more important in shallow coastal waters with high water clarity (11). Complementary to ALB, the mapping of observed NRCS modulation signatures due to sea bottom topography is a useful tool in oceanography and marine geology of coastal waters with strong tidal currents independently of the concentration of water constituents. However, it has been shown that a reduction of background NRCS from SAR is found highly correlated with the increase of Sea-viewing Wide Field-of-view Scanner (SeaWiFS) Chlorophyll-a (Chl-a) concentration (12). An overview of general spatial scales of bedforms and ocean floor topography as a function of water depth by using different remote sensing radar systems was presented by (13). Imaging radars are used for the detection of tidal current ridges, sand waves, and other morphological changes of the sea floor in water depths ≤ 50 m. The private company ARGOSS in the Netherlands has developed a new depth monitoring system (two-dimensional version of the Bathymetry Assessment System (BAS-2D)), for mapping water depths of shallow coastal waters based on SAR observations and echo sounding data (14,15). A technique by rewriting classical physical models as a series of non-linear filters using Volterra models was presented by (16). They demonstrated by using such a technique that the inversion algorithm avoids the use of an iterative data assimilation scheme. Their method is based only on the physical knowledge of the imaging mechanism that is expressed by the so called Volterra kernels.

However, the study of radar signatures in coastal waters described by (17) also demonstrated the critical nature that topographic and stratified effects could have via the associated hydrodynamics for the interpretation of radar imagery. Radar signatures of internal waves superimposed on surface manifestations caused by the seabed have been presented by (18). The influence of quasi resonant internal waves on the radar imaging mechanism of shallow sea bottom topography was discussed by (19). Therefore, the question of whether the water column in any coastal area is vertically well mixed and stratification can be neglected when discussing the NRCS modulation caused by the sea floor has to be carefully investigated, too. Other oceanographic phenomena like frontal boundaries, small scale eddies, slicks, oil spills, patches of turbulence and ship wakes are quite common in coastal waters and can also disturb the radar signatures of the seabed.

EXPERIMENT AND MEASUREMENT CONFIGURATION

The first field experiment of the *Operational Radar and Optical Mapping* in monitoring hydrodynamic, morphodynamic and environmental parameters for coastal management (OROMA) project of the Fifth Framework Programme of the European Commission (EC) was carried out from 5 to 16 August 2002. The study area is the Lister Tief, a tidal inlet of the German Bight in the North Sea bounded by the islands of Sylt to the south and Rømø to the north, respectively, as shown in Figure 1. Two institutes have participated: the GKSS-Research Centre, Institute for Coastal Research, Geesthacht, Germany and the GEOMAR Research Centre for Marine Geosciences at the University of Kiel, Germany. In the following, the measurements performed on board the Research Vessel (R.V.) *Ludwig Prandtl* of GKSS are mainly described.
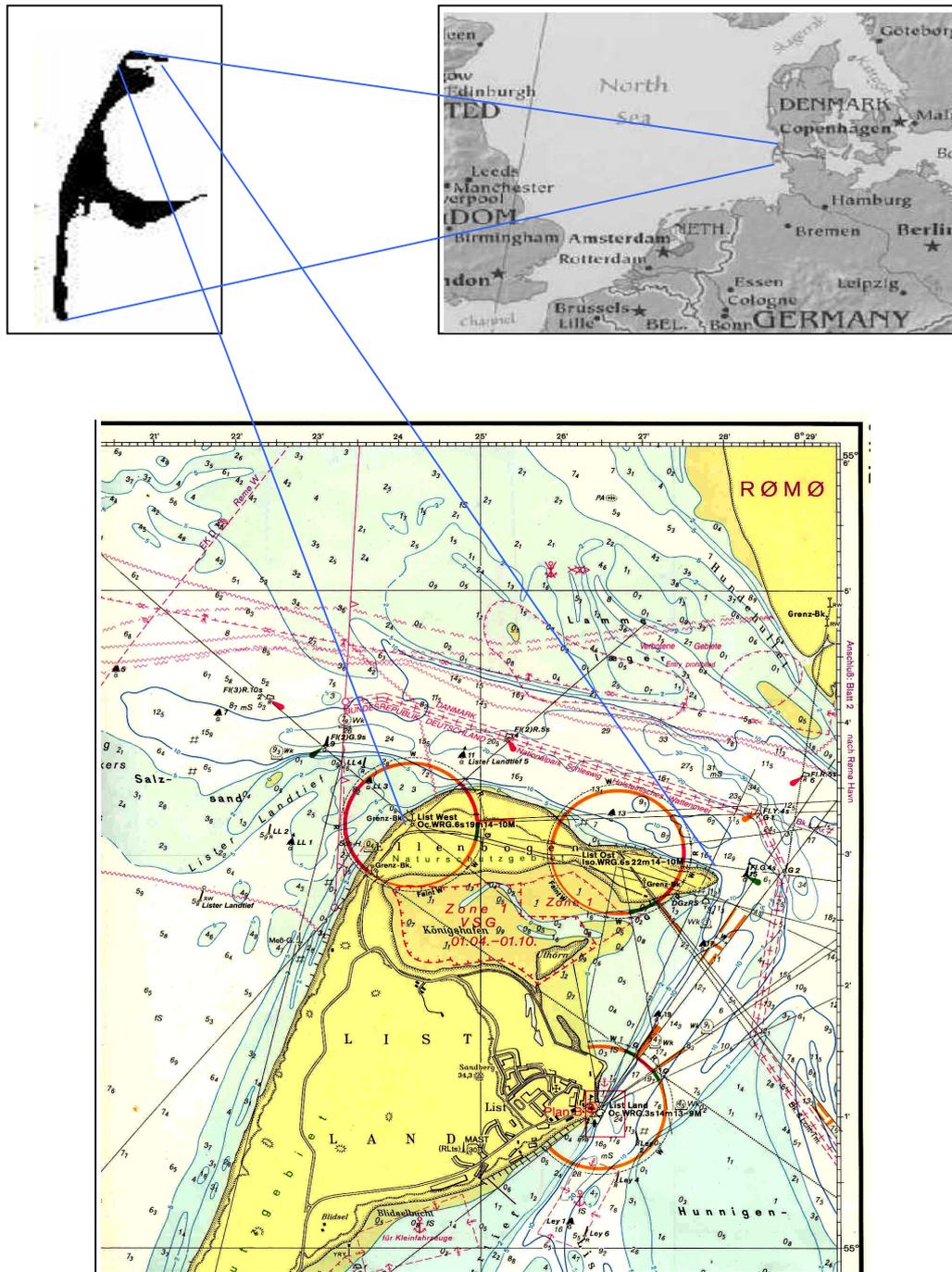
Figure 1: Location and bathymetry of the Lister Tief in the German Bight of the North Sea.

The Lister Tief was selected because one of the most pronounced and dynamic sand wave fields in German coastal waters is located in this tidal channel. The R.V. *Ludwig Prandtl* was equipped with the following sensors which have been used and operated during the OROMA experiment: a NAVISOUND 2000 echo sounder with a frequency of 210 kHz, a TRIMBLE Nav Beacon DSM 212 Differential Global Positioning System (DGPS) with a data rate of 1 s, an RD Instruments Acoustic Doppler Current Profiler (ADCP) with a frequency of 1200 kHz, a Kelvin Hughes RSR 1000 X-band VV polarized river radar, a Siggelkow Gerätebau GmbH Soni 3 meteorological sensor system with a data rate of 6 s, a ME Ecosonde Conductivity-Temperature-Depth (CTD) probe, and handheld cameras. The measurement configuration on board R.V. *Ludwig Prandtl* is shown in Figure 2.
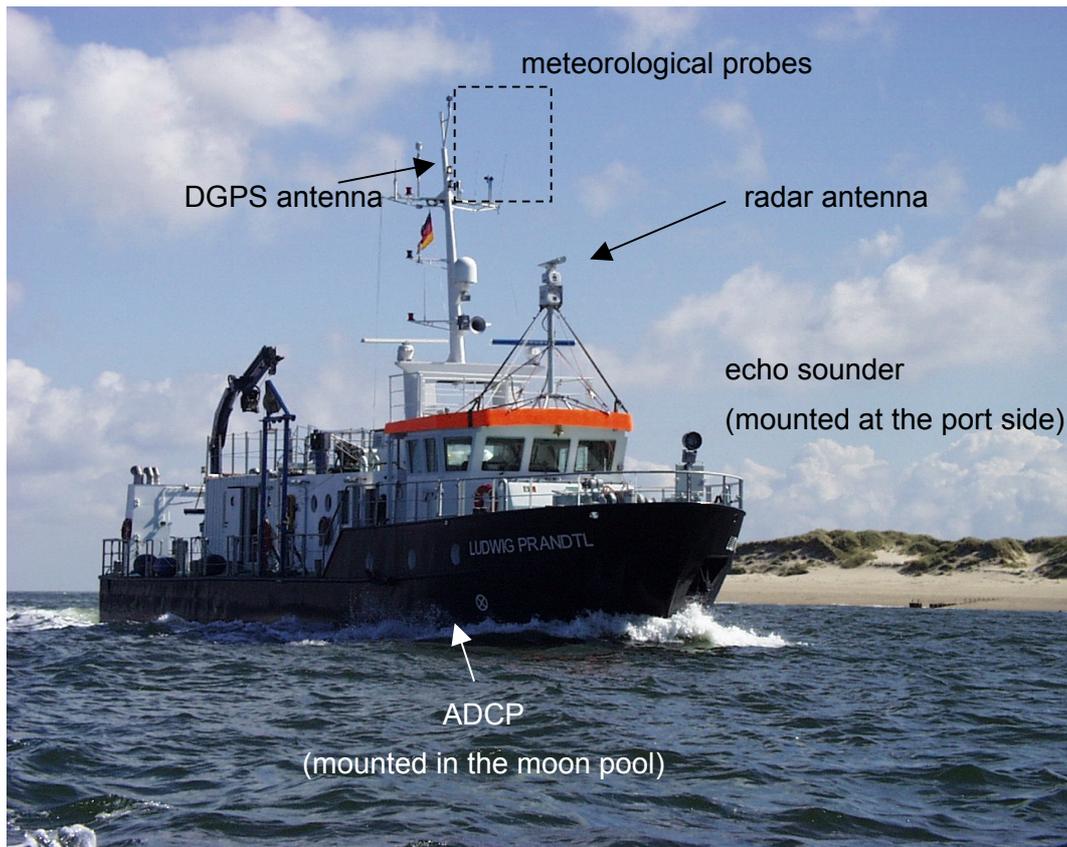
Figure 2: Measurement configuration on board Research Vessel (R.V.) Ludwig Prandtl used in the Lister Tief during the OROMA experiment on 14 August 2002.

Almost all surveying profiles of the ADCP measurements across the study area were obtained on board R.V. *Ludwig Prandtl* at a ship speed between 1.5 m s^{-1} and 2.5 m s^{-1}. The ADCP was mounted within the moon pool of the ship at 1.7 m water depth. An arrangement of 4 downward-looking convex transducers was installed in such a way that 2 pairs of transducers pointed in the fore-aft and starboard-port directions, respectively, with an incidence angle of 20°. Three transducers were required to compute the three dimensional current velocity field (e.g. north, east, and vertical). The redundant information of the fourth transducer was used by the system to compute the error of the current velocity and to evaluate whether the assumption of horizontal homogeneity was reasonable enough during the experiment. Separate digital water depth data of lower spatial resolution were also measured by the ADCP in addition to the water depth measurements obtained by the echo sounder. The flow velocity and water depth measurements were recorded continuously from a water depth of 2.32 m downward to the seabed, separated into water depth cells (bins) of 0.25 m. The collected and processed data after each pulse transmission were averaged over a sampling interval of 5 seconds. At the end of the sampling interval, a profile of the resulting current velocity relative to the ADCP was generated as a function of range and then stored on the hard disk of the connected computer. The relative accuracy of the current velocity is ±1 cm s^{-1} and the accuracy of the estimated absolute current velocity is ±5 cm s^{-1}.

RESULTS

Seabed morphology

Significant new information detected from marine remote sensing radar imagery such as SEASAT SAR images was that the angle between tidal current ridges and maximum current velocity was between 10^0 and 20^0. This was observed due to the presence of parallel roughness streaks on the sea surface induced by the tidal current (20). Radar images of sea bottom topography confirm that sand waves, as they approach the crest of a tidal current ridge, do not maintain their crestlines at

approximately normal to the general direction of peak tidal flow but bend around to become tangential to the crest of the ridge. RAR images of the southern North Sea analysed by (21) showed that sand waves which are superimposed on tidal current ridges change orientation and character abruptly at the crest. The behaviour of tidal current directions due to the presence of submarine sand waves was discussed by (22). They calculated from the components of the surface current velocity a direction change of the tidal flow between 5° and 33°.

One of the major challenges of morphodynamic modelling is the consideration of different scale interactions of tidal current ridges or linear sand banks, sand waves, and (mega) ripples (23). A hierarchy of superimposed bedforms on a sand ridge ranging from linguoid ripples, small sand waves, and up to large sand waves has been published by (24). The analysis made by (25) in the southern North Sea has revealed a new regular pattern labelled as long bed waves, in addition to the well-known sand waves and tidal current ridges. These long bed waves have also been observed already on SEASAT SAR imagery in 1978 and little attention was paid to them at that time.
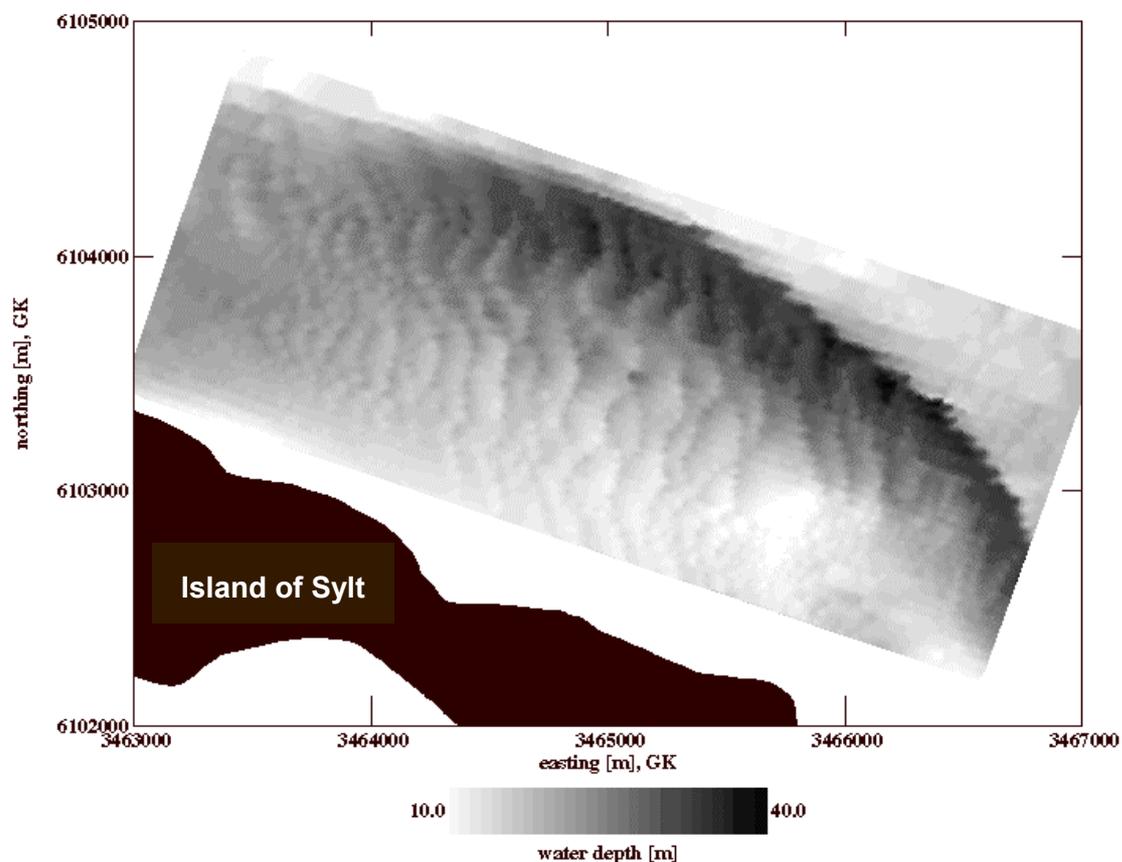

Figure 3: Pre-processed map of the sea bottom topography of the whole study area in the Lister Tief as recorded by the NAVISOUND 2000 echo sounder in combination with a DGPS system during the OROMA experiment in August 2002. The data have been interpolated onto a grid of 20 m by 20 m and are visualized in a map based on Gauss-Krüger-Coordinates. The profile of the analysed ADCP measurements shown in Figure 9 is also included as the red line. The black area is the northern part of the island of Sylt.

In this section, the interaction between large asymmetrical sand waves (spacing: 200-500 m) with large lee slopes and associated mega ripples (spacing: > 1 m) located in the troughs of the sand waves will be especially outlined. A pre-processed map of the sea bottom topography of the whole study area in the Lister Tief as recorded during the OROMA experiment in August 2002 is shown in Figure 3. Sounding tracks at 50 m distances were gathered by the NAVISOUND 2000 echo sounder in combination with a DGPS system. The transducer system of the NAVISOUND 2000 echo sounder system was installed at the port side of R.V. *Ludwig Prandtl* at a distance of 20 m from the bow of the ship. The data triplets (x, y, z), with x and y the two horizontal coordinates and

z the vertical coordinate, respectively, have been interpolated onto a grid of 20 m by 20 m and is visualized in a map based on Gauss-Krüger-Coordinates in Figure 3. The coverage is 3850 m by 1350 m. A noisy interrupted feature of a large water depth change of a submarine terrain edge ranging from 34 m to 14 m is visible in the north-eastern part of the study area. This is due to the applied interpolation technique. But these data will not be considered for further analysis. The profile of the analysed ADCP measurements (see below) is also included in Figure 3.

The seabed morphology of the Lister Tief tidal channel is a complex configuration of different bedforms. The sand waves investigated in this study are four-dimensional in space and time. Small scale as well as megaripples are superimposed on sand waves (see Figure 4). The sand waves have heights $\leq$ 11 m and often crest to crest distances (spacings) > 300 m. In the past, systematic morphological investigations have been carried out to study the migration of these sand waves (26). In the northern section of the test area most of the sand waves have ebb tide oriented forms; in the southern part most of them are flood tide oriented. In the southeastern part the stoss slopes of sand waves are of the order of $\partial z/\partial x \leq 0.017$. The lee slopes have maximum values of $\partial z/\partial x = 0.591$. Sand waves with a mean height of 3 m migrate about 60 m per year. This migration of sand waves is caused by the local current regime. During each tide a water volume of about $5.25 \cdot 10^8$ m^3 passes through the tidal channel, which is bound by the islands of Sylt to the south and Rømø to the north. These islands are connected by dams to the mainland and therefore the Lister Tief is the entrance of an artificial tidal bight.
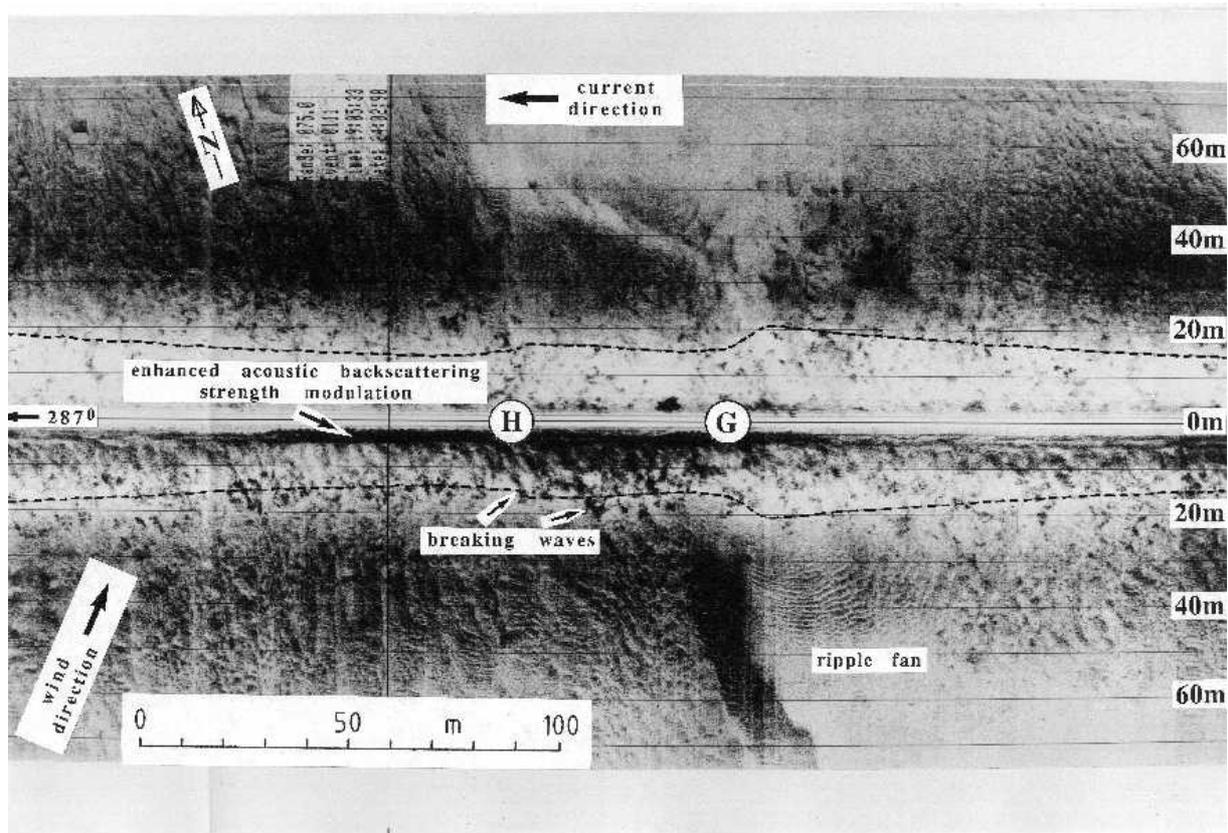

Figure 4: Side-scan record of the 500 kHz sonar system Klein 595 in the sea area of the Lister Tief on 24 February 1990 at 18:05 UTC during ebb tidal phase (28). G and H indicate the location of sand wave crests. Enhanced acoustic backscatter is shown by dark signatures. Low acoustic backscatter and shadow zones are presented by bright signatures. The broken lines indicate the water depth profiles below the towed sonar fish. The mean wind and current directions are shown by arrows.

It has been shown by (27) that the orientation of the crestlines and the separation between crests of the sand waves varied according to their position in the field. They showed that the two sectors in which the sand wave field has been divided were almost perfectly separated by bifurcations of the crestlines. The observation of megaripple fans is associated with a large angle of the lee flank and an arcuate orientation of the sand waves (27,28). Such a megaripple fan located in the trough of a sand wave is imaged in Figure 4 showing a side-scan record of the 500 kHz sonar system Klein 595 in the sea area of the Lister Tief on 24 February 1990, at 18:05 UTC during the ebb tidal phase (28). The wind speed was 10 m s^{-1} and the direction was from 220°. Two crests of sand waves are marked by G and H. The enhanced acoustic backscattering strength modulation associated with breaking waves was caused by these two bedforms. The location of this megaripple fan coincided with those stations where both strong horizontal and vertical current shear have been observed (9). Similar sand waves with large slopes on their lee flanks have been also noticed in the Malacca Strait, Southeast Asia (29). It is considered that the formation of megaripple fans is due to flow separation at the crest of the sand waves. This mechanism is confirmed by the existence of turbulence patterns at the water surface. The position of such patterns was observed near the crests of sand waves. Similar observations have been made in the Brahmaputra river by (30). Figure 5 shows a picture of turbulence patterns at the sea surface observed near the crests of flood orientated sand waves in the sea area of the Lister Tief. This handheld camera image was acquired from on board the R.V. *Ludwig Prandtl* on 15 August 2002 at 15:19 UTC during the flood tidal current phase. At that time the wind speed was 2-3 m s^{-1}.
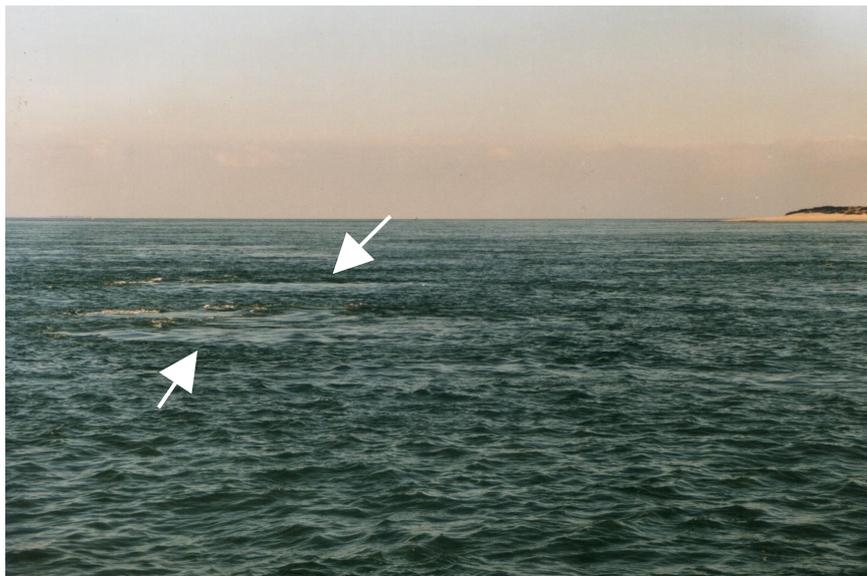

Figure 5: Handheld camera picture of turbulence patterns (marked by arrows) in the sea area of the Lister Tief acquired from on board the R.V. Ludwig Prandtl *on 15 August 2002 at 15:19 UTC during the flood tidal current phase.*

General meteorological and oceanographic observations

Meteorological data were been measured on board R.V. *Ludwig Prandtl* during all recorded vertical profiles of the surveying on 5-16 August 2002 in the OROMA study area of the Lister Tief. The measurements were gathered every 6 seconds at a height of 12 m above the water surface. The data of the sea surface height ζ, which are related here to the chart datum of Normal Null (NN) were measured by the tide gauge station at List on the island of Sylt and were provided by the Amt für Ländliche Räume, Husum, Germany. The Tide gauge station List is located 5 km southerly of the study area. The data measured on 10 August 2002 were selected because detailed ADCP measurements have been carried out in an area of large flood orientated sand waves.
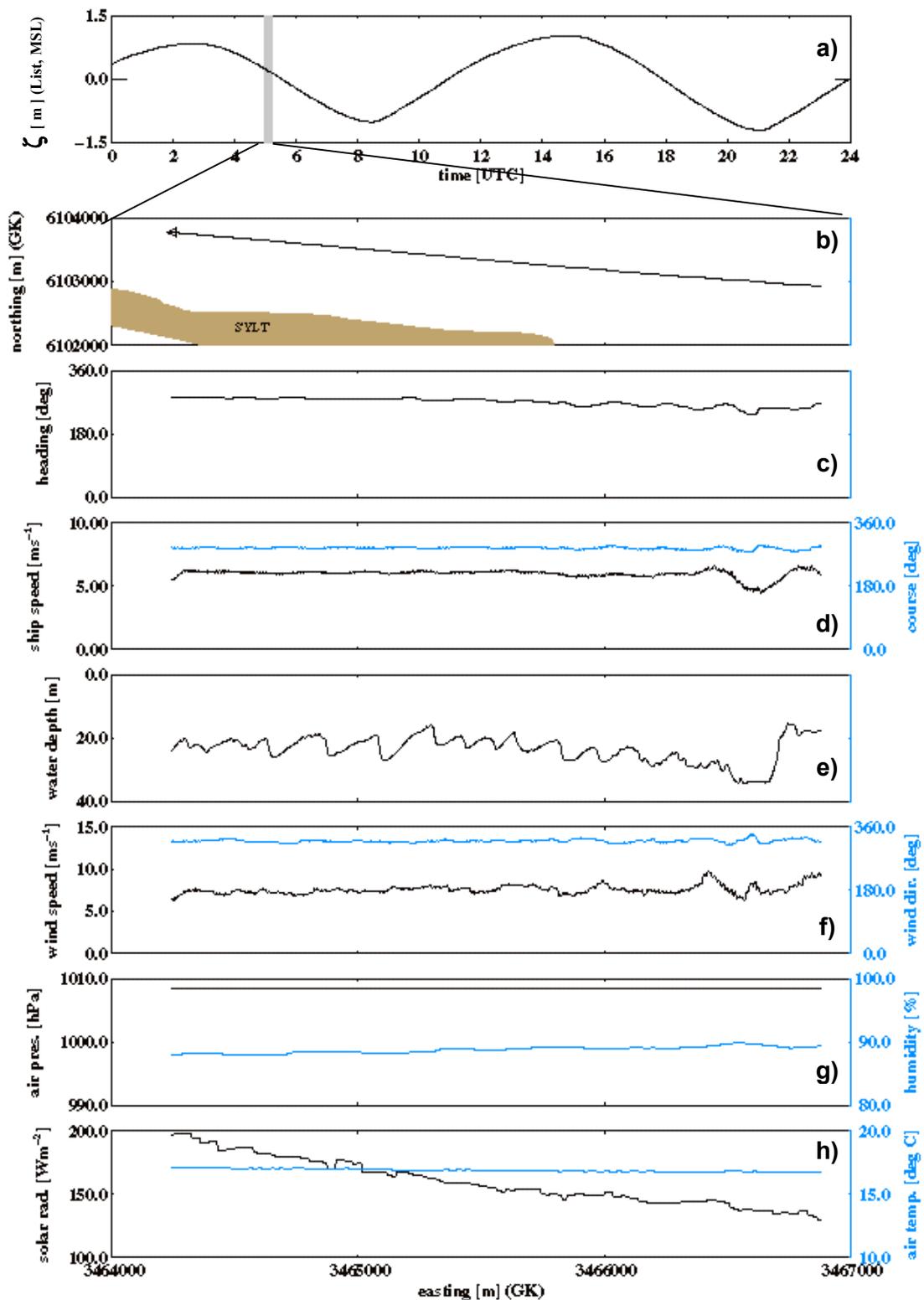
Figure 6: a) Time series of sea surface height ζ on 10 August 2002 between 00:00-24:00 UTC from tide gauge data at List station on the island of Sylt (brown shaded in b)). The following spatial series (in Gauss-Krüger-Coordinates) of meteorological, oceanographic, and other relevant data of the OROMA study area Lister Tief have been measured on board R.V. Ludwig Prandtl *on 10 August 2002, 05:00-05:15 UTC, during ebb tidal current phase: b) location of the analysed profile, c) heading, d) ship speed and course, e) water depth, f) wind speed and direction, g) air pressure and humidity, and h) solar radiation and air temperature.*

Figure 6a shows a time series of ζ on 10 August 2002 between 00:00-24:00 UTC. The dominant signal of the sea surface height is the period of the semidiurnal M2 tide. The extrema of the amplitudes vary between -1.15 m $\leq \zeta \leq$ 1.04 m. The grey shaded time window between 05:00-05:15 UTC in Figure 6a indicates the time period of the other measurements shown in Figures 6b-h. During that time interval of 15 minutes sea surface heights between 0.12 m and 0.23 m were measured. Figures 6b-h show spatial series of several measured meteorological and hydrographic parameters. The location of the analysed profile in an area of flood dominated sand waves is presented in Figure 6b. The display values of the gyro compass shown in Figure 6c vary between 263° and 284° in the western part of the profile. These data are needed as input data for the ADCP and the radar system. The ship speed was 5.8 m s^{-1} and the ship course 287° (see Figure 6d), respectively. Figure 6e shows the water depth with a series of flood dominated asymmetric sand waves. The water depth varies between 15.38 and 33.08 m during the whole profile. The large sand waves in the western part of the profile have crest to crest distances of about 240 m and maximum heights of 11 m. Wind speeds of 6.3 m s$^{-1} \leq U_w \leq$ 9.8 m s^{-1} with a mean direction coming from 320° (westerly direction) have been measured and are presented in Figure 6f. Figure 6g shows the observations of a mean air pressure of 1008 hPa and a mean humidity of 89%, respectively. An increase of the solar radiation from 130 W m^{-2} at the beginning of the profile to 200 W m^{-2} at the end is associated with a constant air temperature of 17°C shown in Figure 6h.

Conductivity-Temperature-Depth (CTD) data measured by the ME Ecosonde on board R.V. *Ludwig Prandtl* are presented in Figures 7a-c. These data were gathered on 10 August 2002 at 08:50 UTC. All three vertical profiles of the water temperature, salinity, and potential density of the CTD probe, respectively, show a weak developed two layer system at a water depth of 1.5 m. The mean water temperature difference ΔT of the upper layer T_1 and the lower layer T_2 is $\Delta T = T_1 - T_2$ = 19.9°C - 19.8°C = 0.1°C. The salinity is more or less constant with 28.5 within the whole water column. The potential density σ_θ has a mean difference between the two water layers of $\Delta\sigma_\theta = \sigma_{\theta 1} - \sigma_{\theta 2} = -0.1$ kg m^{-3}. This analysis shows that the water column in this coastal area is vertically well mixed at that time and the weak observed stratification can be neglected for the radar imaging mechanism of submarine sand waves.
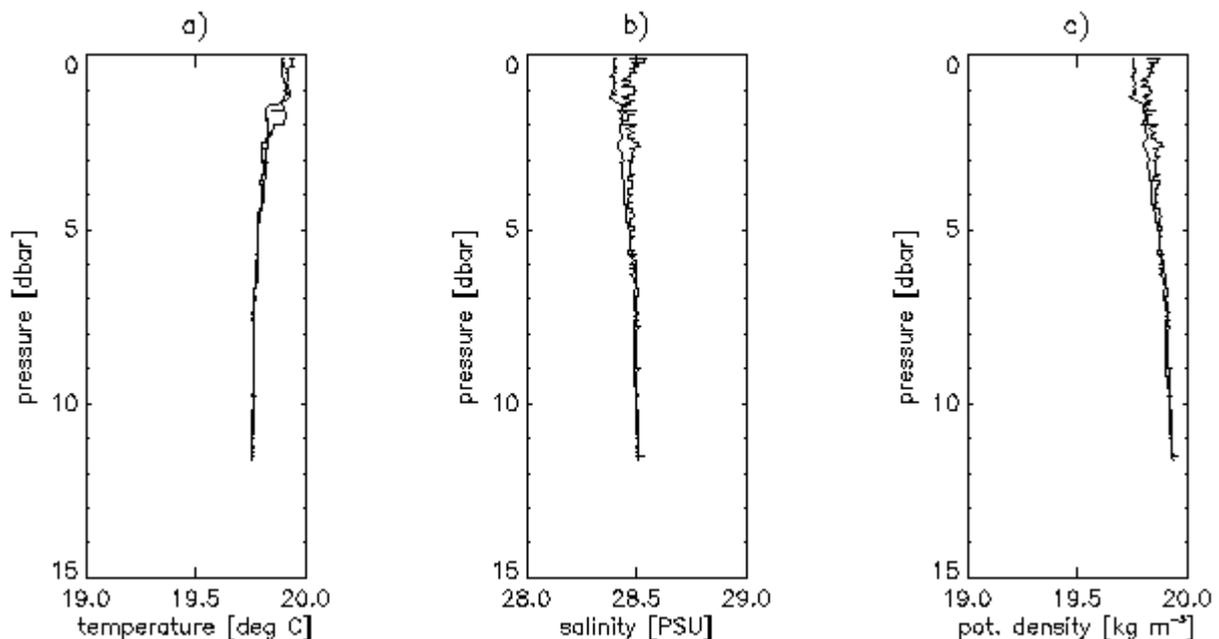

Figure 7: Vertical profiles of Conductivity-Temperature-Depth (CTD) data measured by the ME Ecosonde in the Lister Tief on board R.V. Ludwig Prandtl on 10 August 2002 at 08:50 UTC; a) water temperature, b) salinity, and c) potential density.

ADCP measurements

In this paper a coordinate system was used where the two-dimensional space variables are de-fined perpendicular x_{perp} and parallel x_{par} to the sand wave crests. This definition is based on the components of the current velocity perpendicular u_{perp} and parallel u_{par} to the sand wave crests, be-cause it has been shown that the gradient of the perpendicular component relative to the sand wave crests of the current velocity $\partial u_{perp}/\partial x_{perp}$ is an important parameter of the radar imaging mechanism of sea bottom topography (2). The definitions of the coordinate system and symbols are shown in Figure 8.
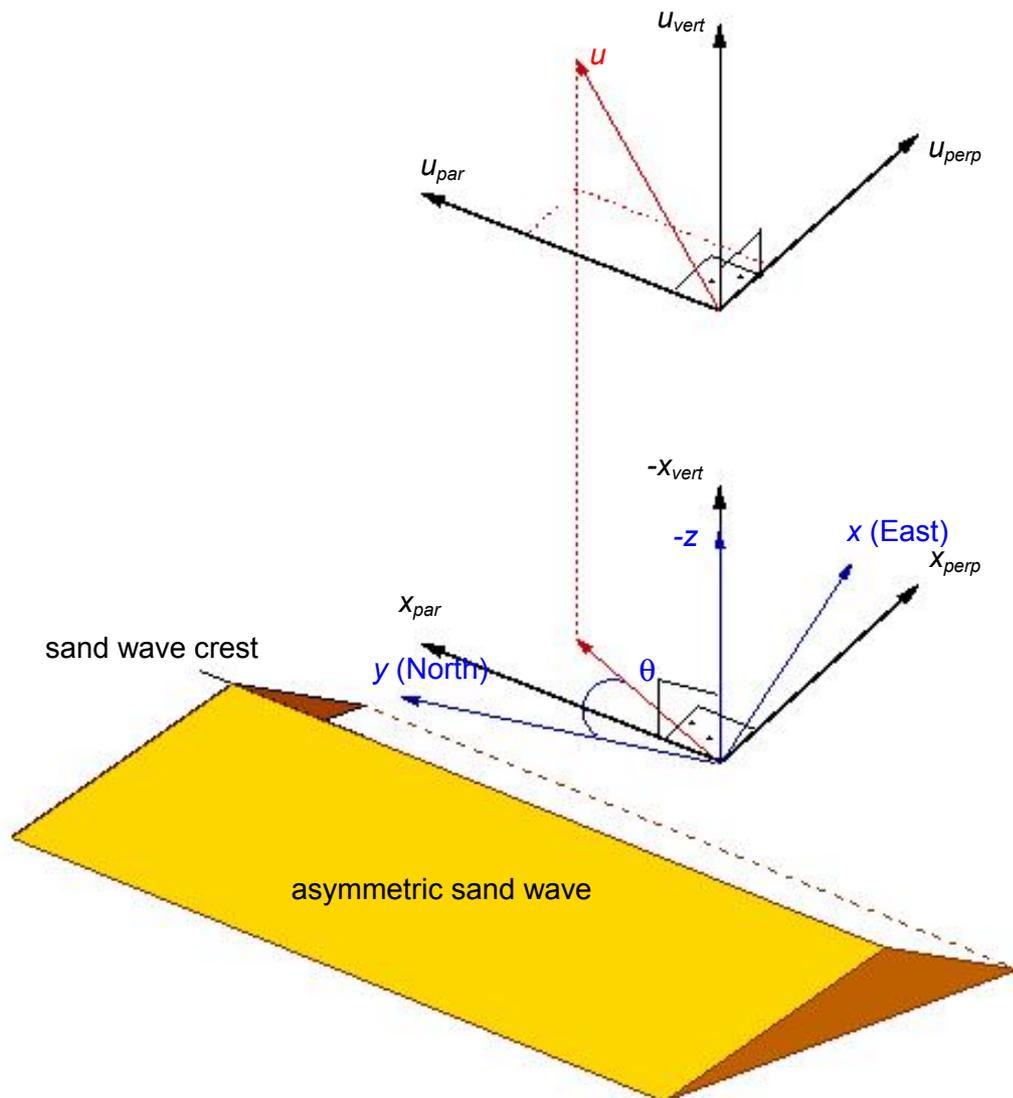
Figure 8: Definition of the used coordinate system and symbols.

Detailed water depth dependent ADCP measurements above asymmetrical flood tide oriented large sand waves were carried out on 10 August 2002 between 05:00-05.15 UTC on board R.V. *Ludwig Prandtl* during the ebb tidal current phase. The analysed section of the profile had a length of 1290 m. These ADCP data and several other calculated parameters are shown in Figures 9a-h as a function of the horizontal space component perpendicular to the sand wave crest x_{perp}. All depth cells (bins) with a vertical spatial resolution of 0.25 m have been considered for the calcula-tion of the current velocity covering the water depths from 2.32 m below the sea surface to 1.2 m above the sea bottom topography. At the interface between the water and the seabed the ADCP data have to be considered with caution due to acoustic interference from the bottom. The water depth measured by the ADCP is coloured in black. Water depth measurements derived by the

NAVISOUND 2000 echo sounder are indicated by a bright line. The slightly different water depth measurements are due to the different positions of the transducer systems on board R.V. *Ludwig Prandtl* and due to the different footprints. All measured ADCP data and calculated parameters shown in Figures 9a-h indicate distinct changes across the track ranging from the near water surface to the sea bed. The most significant variations of all parameters are related to the crests of the sand waves. A mean current speed of the perpendicular component relative to the sand wave crest of the current velocity $u_{perp\ mean}$ = 90 cm s^{-1} was calculated from the measurements of all bins during the observation period and is shown in Figure 9a. Maximum current speeds were measured at the crests of sand waves and minimum current speeds at the troughs of sand waves, respectively. Figure 9a reveals that almost all sand waves cause significant changes up to 40 cm s^{-1} in u_{perp} as a function of x_{perp} and the water depth. Figure 9b shows the distribution of the parallel component u_{par} relative to the sand wave crest of the current velocity above the sand waves. A mean current speed of $u_{par\ mean}$ = 30 cm s^{-1} was calculated from the measurements of all bins. Again all sand waves cause significant changes up to 60 cm s^{-1} in u_{par}. The parallel component u_{par} decreases from the near water surface to the seabed. The vertical component u_{vert} of the current velocity as a function of x_{perp} and the water depth is presented in Figure 9c. Minimum and maximum values of -10 cm s$^{-1} \le u_{vert} \le 6$ cm s^{-1} have been derived from the ADCP data. Marked waterspouts of the direct upward orientated vertical component of the current velocity have been developed at the crests of sand waves. The downward orientated vertical component is located at the troughs and gentle slopes of the sand waves. A regular structure of circulation cells of u_{vert} within the water column was developed during that time of the tidal phase caused by the undulations of the seabed. These waterspouts created by u_{vert} causes the turbulence patterns at the water surface shown in Figure 5. The upward orientated patterns of u_{vert} are superimposed with the divergent zones of $\partial u_{perp}/\partial x_{perp}$ presented in Figure 9e.

The direction of the surface current velocity θ relative to changes of the seabed is shown in Figure 9d. A direction change $\Delta\theta$ up to 60° was calculated from the components of the current velocity presented in Figures 9a-b. The perpendicular and parallel components of the current velocity shown in Figures 9a-b are related to the variation of the direction of the current velocity. The strain rate or the gradient of the perpendicular component relative to the sand wave crest of the current velocity $\partial u_{perp}/\partial x_{perp}$ is shown in Figure 9e. This image shows the typical distribution of divergent and convergent flow patterns associated with asymmetrical sand waves and confirms the theory developed by (2). Minimum and maximum values of the strain rate of -0.006 s^{-1} and 0.004 s^{-1} have been calculated. Note, that the convergent zones are associated here with a positive sign and the divergent zones with a negative sign, respectively, due to the definition of the negative direction of $-u_{perp}$ (ebb tidal current direction). Comparable magnitudes of ±0.006 s^{-1} have been calculated for the shear of the parallel component of the current velocity relative to the sand wave crests $\partial u_{par}/\partial x_{perp}$ shown in Figure 9f. The shear of the vertical component of the current velocity $\partial u_{vert}/\partial x_{perp}$ is presented in Figure 9g and varies between -0.003 s$^{-1} \le \partial u_{vert}/\partial x_{perp} \le 0.002$ s^{-1}; $(\partial u_{vert}/\partial x_{perp})_{max}$ is positioned above the troughs of sand waves and $(\partial u_{vert}/\partial x_{perp})_{min}$ is positioned above the crests of sand waves, respectively. Figure 9h presents the gradient of the direction of the current velocity $\partial\theta/\partial x_{perp}$. Magnitudes of $-0.4°$ m$^{-1} \le \partial\theta/\partial x_{perp} \le 0.6°$ m^{-1} have been calculated. The gradient of the bending of the current direction changes sign at the slopes of the sand waves.

Figure 9a-h shows detailed Acoustic Doppler Current Profiler (ADCP) measurements from the near water surface to the sea bed as a function of the horizontal space component perpendicular to the sand wave crest x_{perp}, obtained on board R.V. *Ludwig Prandtl* during ebb tidal phase on 10 August 2002 during 05:00-05:15 UTC.
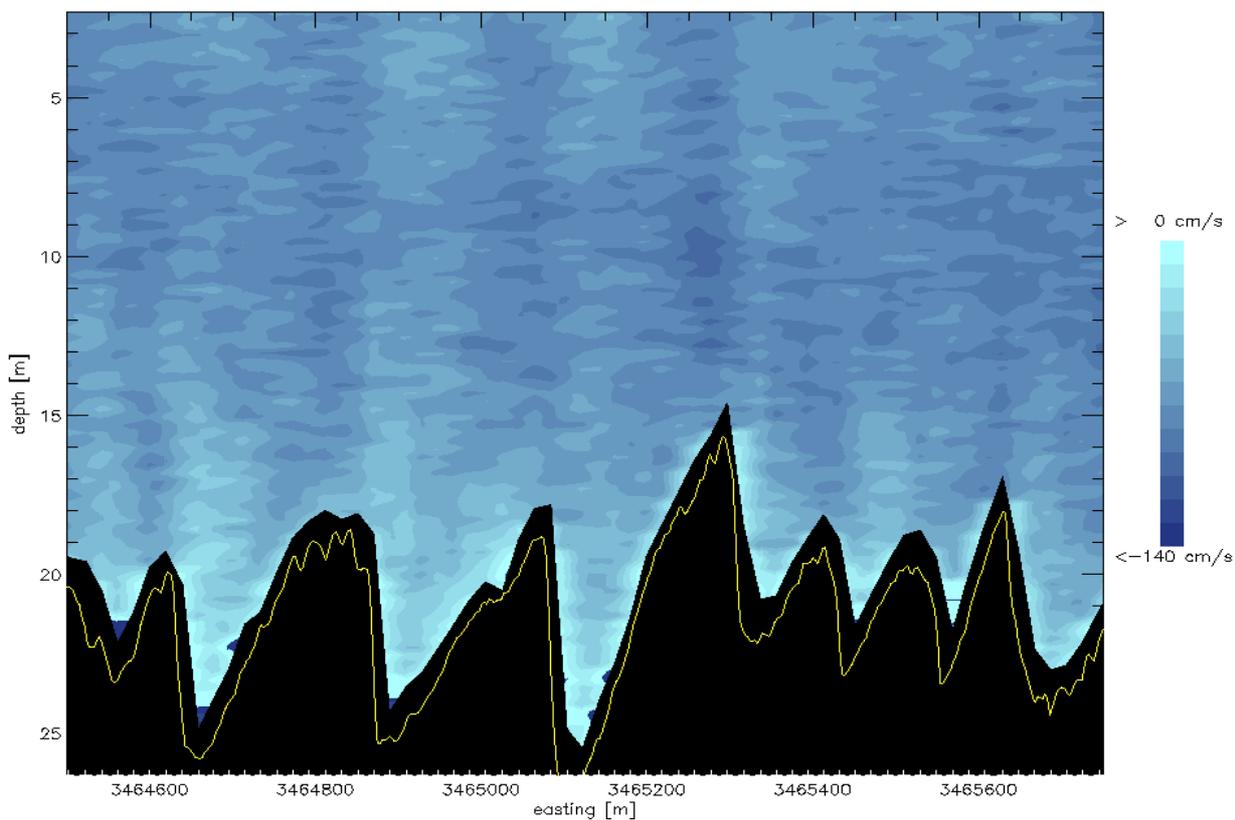
Figure 9a: Perpendicular component u_{perp} *of the current velocity relative to the sand wave crest.*
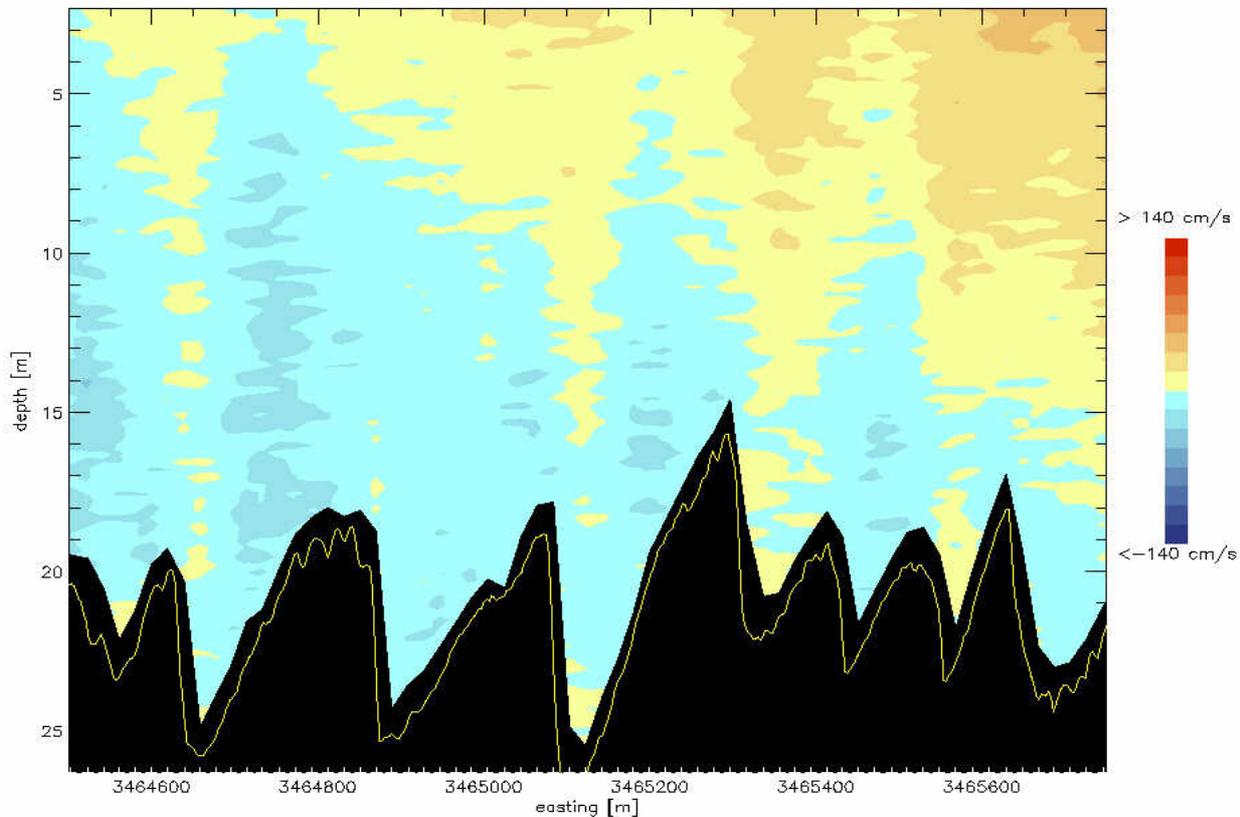

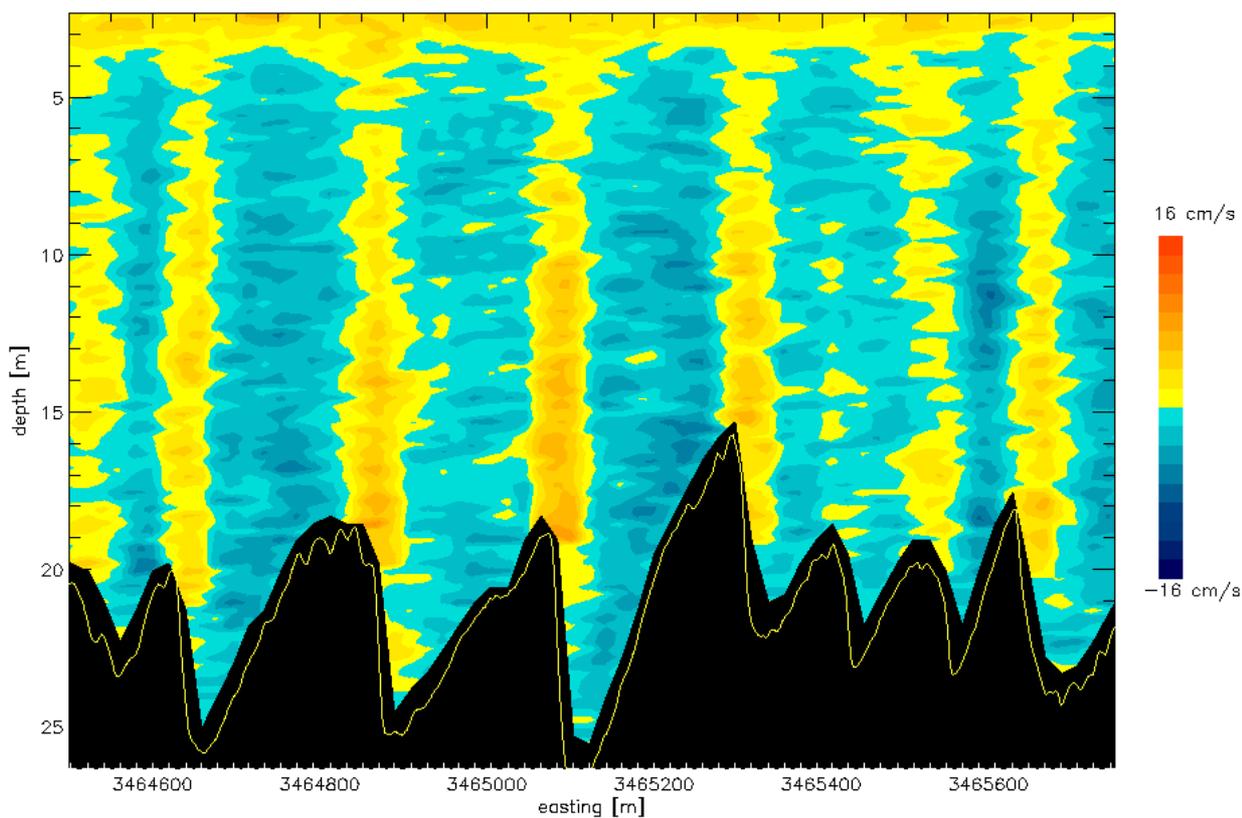*Figure 9b: Parallel component* u_{par} *of the current velocity relative to the sand wave crest.*

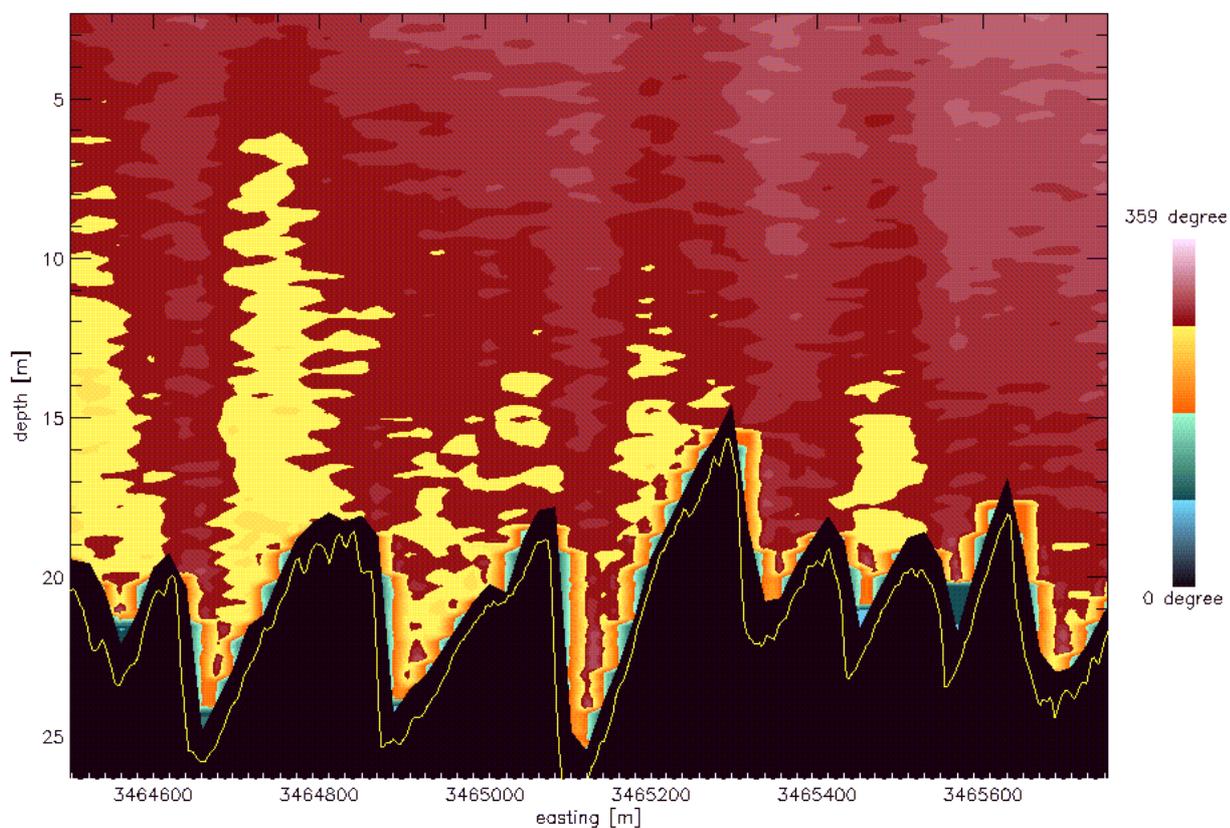*Figure 9c: Vertical component* u_{vert} *of the current velocity.*

Figure 9d: Direction θ *of the current velocity.*

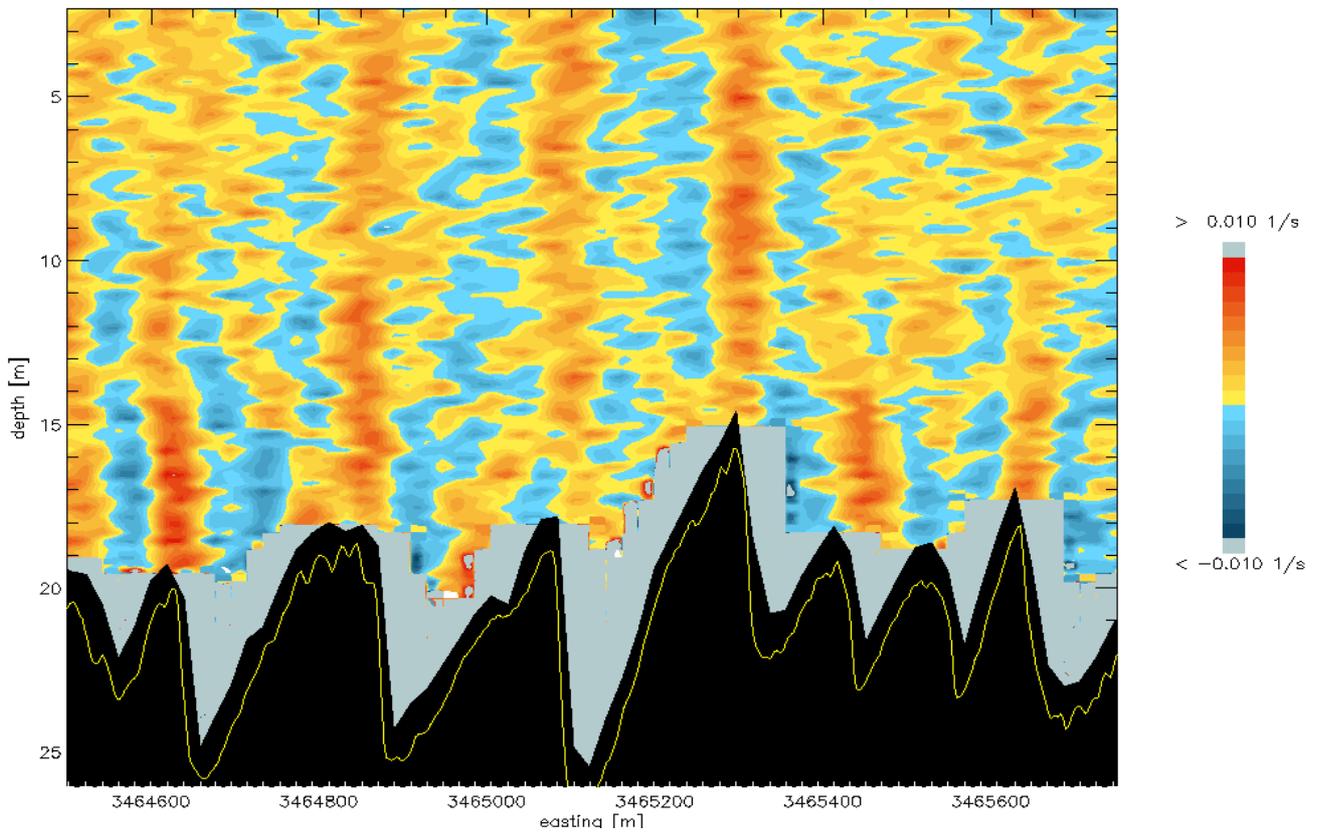*Figure 9e: Gradient of the perpendicular component $\partial u_{perp}/\partial x_{perp}$ of the current velocity relative to the sand wave crest.*
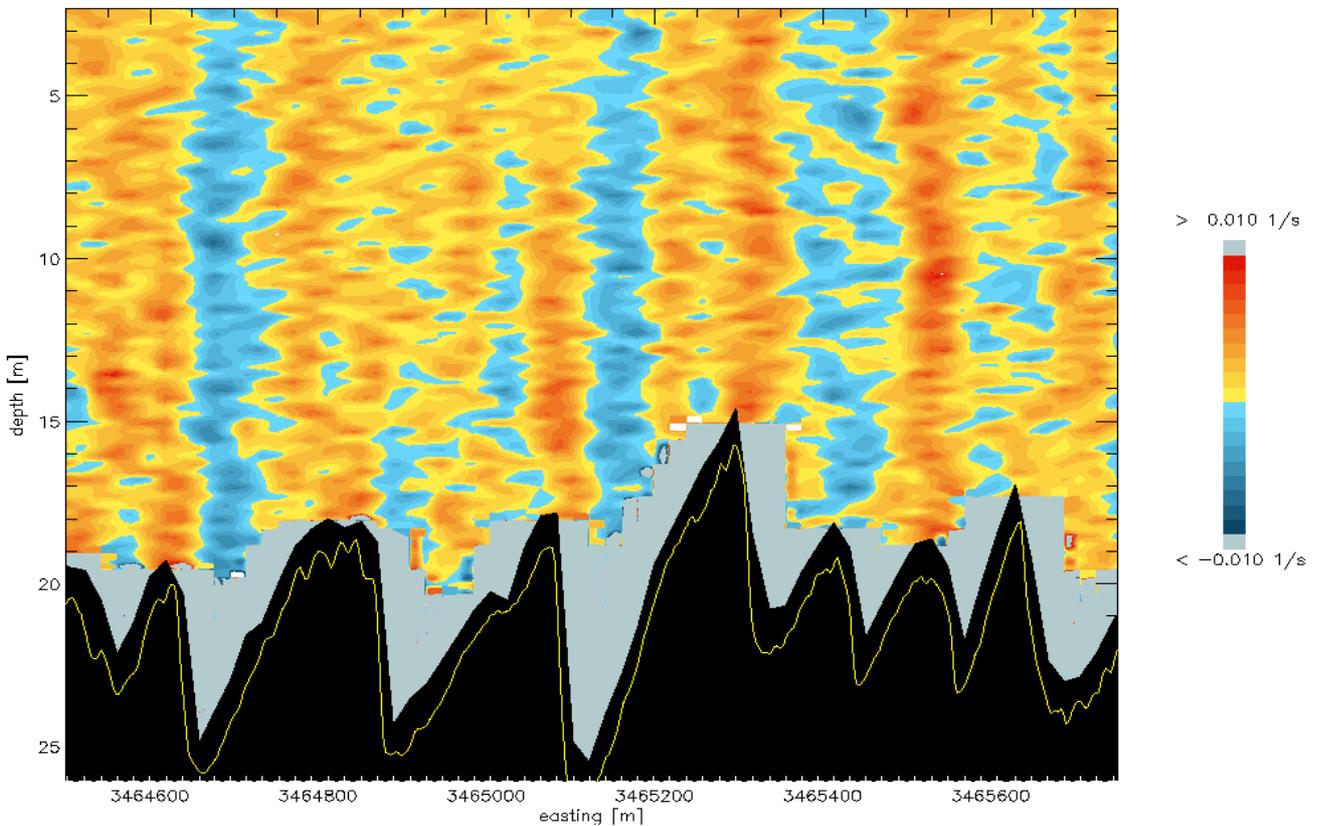

Figure 9f: Gradient of the parallel component $\partial u_{par}/\partial x_{perp}$ of the current velocity relative to the sand wave crest.
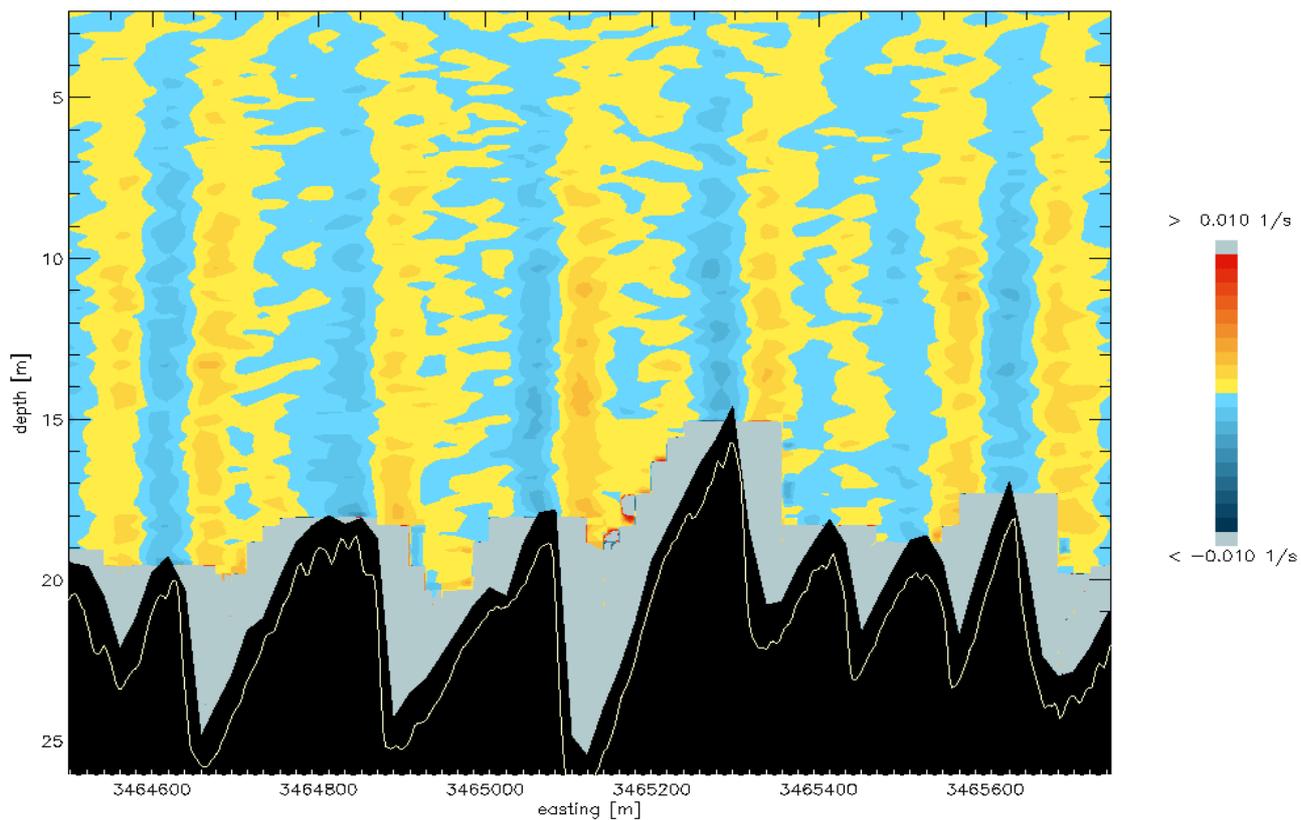
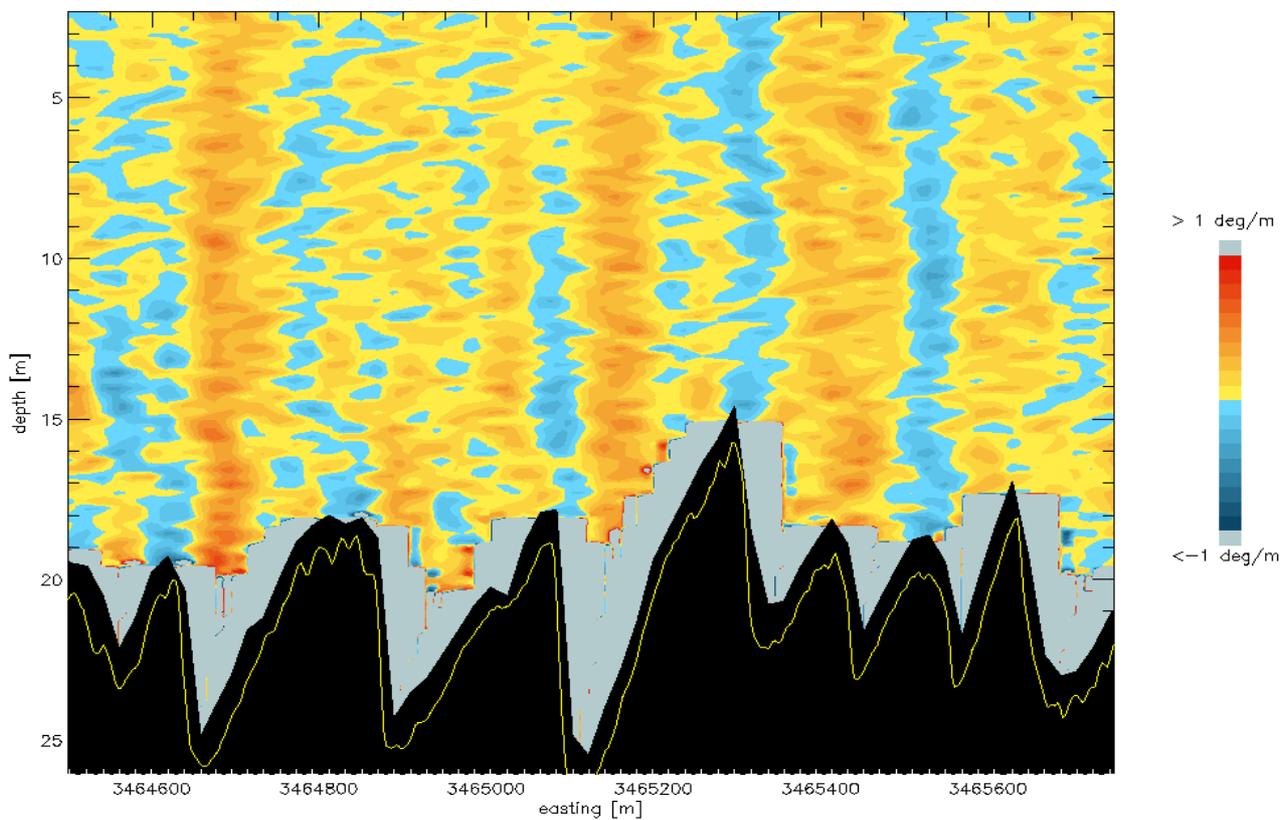*Figure 9g: Gradient of the vertical component $\partial u_{vert}/\partial x_{perp}$ of the current velocity.*

Figure 9h: Gradient of the direction $\partial\theta/\partial x_{perp}$ of the current velocity.

Shipborne radar data

The shipborne coastal monitoring radar of GKSS is based on a Kelvin Hughes RSR 1000 X-band VV polarized river radar and was mounted on board the R.V. *Ludwig Prandtl* during the OROMA experiment on 5-16 August 2002 in the Lister Tief. The extensive radar data analysis is still in progress. As an example, a composite of five single sea clutter images taken by the GKSS shipborne X-band HH-polarized Wave Monitoring Radar (WMR) on 22 November 1990 between 11:45-12:05 UTC is shown in Figure 10 in the sea area of the Lister Tief during a flood tidal current phase. At the time of acquisition the radar composite a mean wind speed of 3.1 m s^{-1} from south-easterly directions was measured. All these radar data are uncalibrated data. The high and low radar return in the Lister Tief shown in Figure 10 are water surface signatures caused by submarine sand waves.
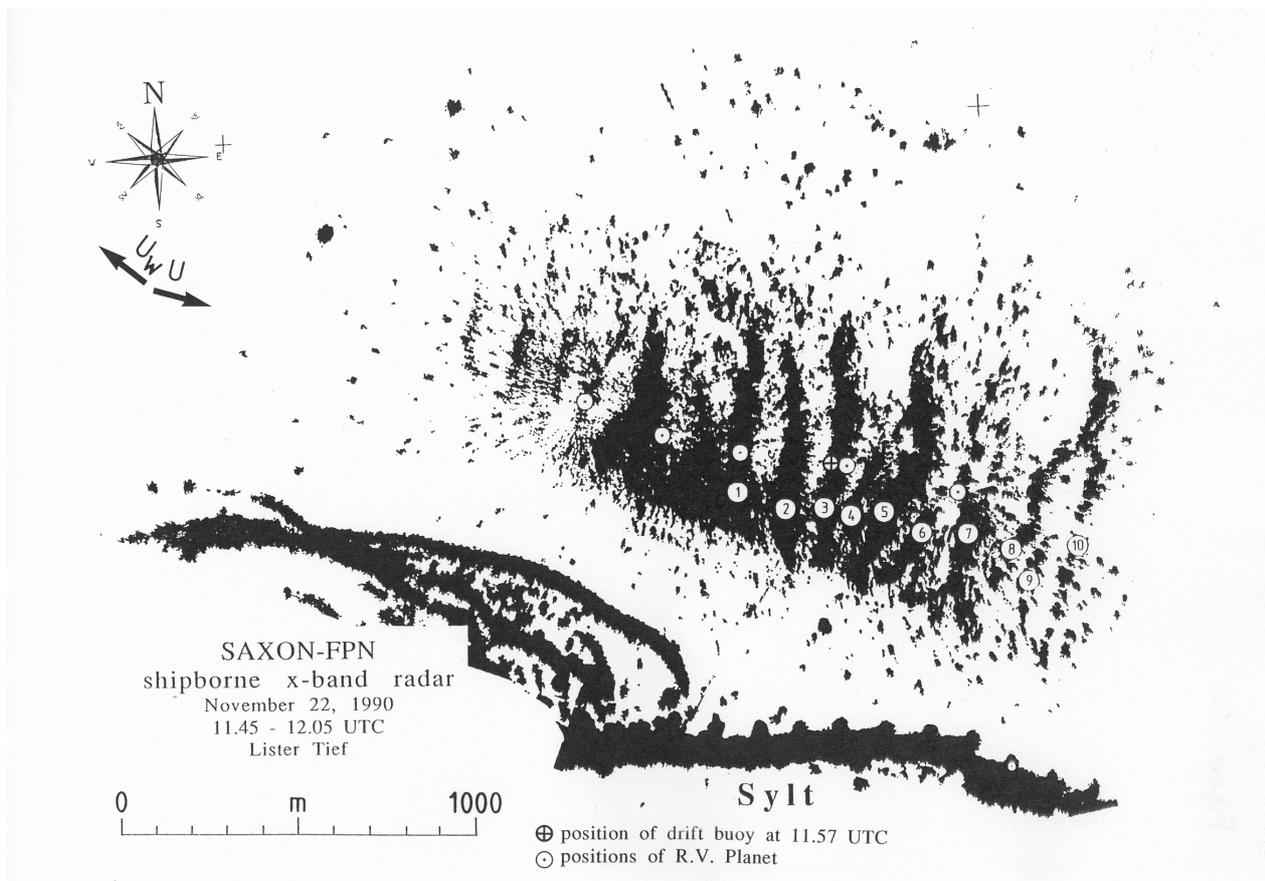

Figure 10: Composite of five single sea clutter images taken by the GKSS shipborne X-band HH-polarized Wave Monitoring Radar (WMR) on 22 November 1990 during 11:45-12:05 UTC in the sea area of the Lister Tief during flood tidal phase. Enhanced radar backscatter is shown by dark signatures. At the time of acquisition of the radar data a mean wind speed of 3.1 m s^{-1} from south-easterly directions was measured. The mean direction of the wind speed U$_w$ and the mean direction of the current U are indicated by two arrows.

The expected progress within the OROMA project will be the availability of calibrated radar data. Normalized Radar Cross Section (NRCS) modulations of the GKSS shipbased X-band radar caused by submarine sand waves will be calculated and mapped in the Lister Tief during ebb and flood tidal current phases. The NRCS modulation data will be made available to the two-dimensional version of the Bathymetry Assessment System (BAS-2D).

DISCUSSION AND CONCLUSIONS

One main aim of the OROMA project is the testing of the BAS-2D tool recently developed by the private company ARGOSS in The Netherlands. It is a new software program for charting the depth of shallow seas by combining information from shipbased X-band VV-polarized radar imagery at low grazing angles and echo sounding data. Careful observations of relevant physical parameters in tidal areas have to be carried out to understand the radar imaging mechanism of sea bottom topography. As it has been shown in this paper there is still a need for experimental quantification to explain all important hydrodynamic processes correctly within the whole water column. Especially users responsible for coastal management have to know how to use and interpret all available data. However, it was demonstrated from the measurements in the Lister Tief that the interpretation of radar signatures of submarine sand waves during special environmental and morphological conditions seems to need more investigations.

The direction change of the surface current velocity θ relative to sand waves was already reported by (31). They described a model for tidal flow over sand waves with its modification in the ebb and flood tidal current phase directions. It was also shown by (22) that if the perpendicular component of the current velocity accelerates then the direction can change anticlockwise significantly up to 33^0 after passing the crests of sand waves in the sea area of the southern North Sea. It is well known that side-scan sonar records show megaripples on one or both sides of the sand waves. The height of the megaripples generally increases in the direction of the sand wave crest. The transit sonar record from the sea area west of Hoek van Holland published by (32) showed as an example that the crestlines of the ripples in the troughs and on both slopes of the sand waves form an angle α_s with the crestline of the sand waves. The angle α_s may reach values up to 45^0 and seems to be a function of the sand wave slope. However, the existence of an angle between the crestlines of megaripples and sand waves indicates that the direction of tidal currents changes also across sand waves. A possible explanation of the current direction variation is that during times of large sand transport the direction of the flow over the sand wave forms an angle with the sand wave crest, generating a bending of flow lines. The resulting current shear produces a torque that also changes the direction of the angular momentum of short waves along their rays at the water surface.

During the OROMA experiment in the Lister Tief the existence of a significant upward orientated vertical component u_{vert} of the three-dimensional current velocity field measured by the ADCP has been shown for the first time. Marked waterspouts of u_{vert} have been measured in a more or less straight line at the crests of asymmetric flood orientated sand waves with large lee slopes. These waterspouts created by u_{vert} produce upwelled water and create turbulence patterns at the water surface. The upward orientated patterns of u_{vert} are simultaneously superimposed on the divergent zones of the perpendicular component relative to the sand wave crest of the current velocity $\partial u_{perp}/\partial x_{perp}$. The downward orientated vertical component of u_{vert} is located at the troughs and gentle slopes of the sand waves. A regular structure of circulation cells of u_{vert} within the water column has been initiated at that time of the tidal current phase. It is considered that the formation of megaripple fans at the troughs of sand waves is due to strong horizontal and vertical current shear as well as developing flow separation at the crest of the sand waves. It is also concluded that the existence of turbulence patterns at the water surface are hints of megaripple fans at the sea bed due to both large slopes as well as arcuate orientations of submarine sand waves.

ACKNOWLEDGEMENTS

REFERENCES

1   De Loor G P, 1981. The observation of tidal patterns, currents and bathymetry with SLAR im-agery of the sea. IEEE Journal of Oceanic Engineering, 6: 124-129

2   Alpers W & I Hennings, 1984. A theory of the imaging mechanism of underwater bottom to-pography by real and synthetic aperture radar. Journal of Geophysical Research, 89: 10529-10546

3   Shuchman R A, D R Lyzenga & G A Meadows, 1985. Synthetic aperture radar imaging of ocean-bottom topography *via* tidal-currents interactions: theory and observations. International Journal of Remote Sensing, 6: 1179-1200

4   Phillips O M, 1984. On the response of short ocean wave components at a fixed wavenumber to ocean current variations. Journal of Physical Oceanography, 14: 1425-1433

5   Hennings I, 1990. Radar imaging of submarine sand waves in tidal channels. Journal of Geo-physical Research, 95: 9713-9721

6   Romeiser R & W Alpers, 1997. An improved composite surface model for the radar backscat-tering cross section of the ocean surface. 2. Model response to surface roughness variations and the radar imaging of underwater bottom topography. Journal of Geophysical Research, 102: 25251-25267

7   Vogelzang J , G J Wensink, C J Calkoen & M W E Van der Kooij, 1997. Mapping submarine sandwaves with multi-band imaging radar 2. Experimental results and model comparison. Journal of Geophysical Research, 102: 1183-1192

8   Zimmerman J F T, 1985. Radar images of the sea bed. Nature, 314: 224-226

9   Hennings I, S Stolte & F Ziemer, 1994. Experimental method to measure surface signature generation by sea bottom undulations. IEEE Journal of Oceanic Engineering, 19: 36-40

10 Hennings I, B Lurin & N Didden, 2001. Radar imaging mechanism of the sea bed: Results of the C-STAR experiment in 1996 with special emphasis on the relaxation rate of short waves due to current variations. Journal of Physical Oceanography, 31: 1807-1827

11 Guenther G C, A Grant Cunningham, P E LaRocque & D J Reid, 2001. Meeting the accuracy challenge in airborne LIDAR bathymetry. EARSeL eProceedings, 1(1): 1-27

12 Lin I-I, L-S Wen, K-K Liu, W-T Tsai & A K Liu, 2002. Evidence and quantification of the corre-lation between radar backscatter and ocean colour supported by simultaneously acquired in situ sea truth. Geophysical Research Letters, 29: 101029/2001GL014039

13 Hennings I , 1998. An historical overview of radar imagery of sea bottom topography. Interna-tional Journal of Remote Sensing, 19: 1447-1454

14 Hesselmans G H F M, G J Wensink, C G Van Koppen, C Vernemmen & C Van Cauwenberg-he, 2000. Bathymetry assessment demonstration off the Belgian coast - BABEL, The Hydro-graphic Journal, 96: 3-8

15 Calkoen C J, G H F M Hesselmans, G J Wensink & J Vogelzang, 2001. The bathymetry as-sessment system: efficient depth mapping in shallow seas using radar images, International Journal of Remote Sensing, 22: 2973-2998

16 Inglada J & R Garello, 2002. On rewriting the imaging mechanism of underwater bottom to-pography by synthetic aperture radar as a Volterra series expansion. IEEE Journal of Oceanic Engineering, 27: 665-674

17 Donato, T F, F Askari, G O Marmorino, C L Trump & D R Lyzenga, 1997. Radar imaging of sand waves on the continental shelf east of Cape Hatteras, NC, U.S.A. Continental Shelf Research, 17: 989-1004

18 Li, X, J Morrison, L Pietrafesa & A Ochadlick, 1999. Analysis of oceanic internal waves from airborne SAR images. Journal of Coastal Research, 15: 884-891

19 Hennings, I, M Metzner, G-P De Loor, 2002.The influence of quasi resonant internal waves on the radar imaging mechanism of shallow sea bottom topography. Oceanologica Acta, 25: 87-99

20 Kenyon N H, 1983. Tidal current bedforms investigated by SEASAT. In: Satellite Microwave Remote Sensing, edited by T D Allan (Ellis Horwood Limited, Chichester), 261-270

21 McLeish W, D J P Swift, R B Long, D Ross & G Merrill, 1981. Ocean surface patterns above sea-floor bedforms as recorded by radar, southern bight of North Sea. Marine Geology, 43: M1-M8

22 Hennings I, B Lurin, C Vernemmen & U Vanhessche, 2000. On the behaviour of tidal current directions due to the presence of submarine sand waves. Marine Geology, 169: 57-68

23 De Vriend H J, 1997. Evolution of marine morphodynamic modelling: Time for 3-D?, German Journal of Hydrography, 49: 331-341

24 Field M E, C H Nelson, D A Cacchione & D E Drake, 1981. Sand waves on an epicontinental shelf: Northern Bering Sea. Marine Geology, 42: 233-258

25 Knaapen M A F, S J M H Hulscher, H J de Vriend & A Stolk, 2001. A new type of sea bed waves. Geophysical Research Letters, 28: 1323-1326

26 Ulrich, J & H Pasenau, 1973. Morphologische Untersuchungen zum Problem der tidebedingten Sandbewegung im Lister Tief, Die Küste, 24: 95-112

27 Aliotta S & G M E Perillo, 1987. A sand wave field in the entrance to Bahia Blanca estuary, Argentina. Marine Geology, 76: 1-14

28 Hennings I, H Pasenau & F Werner, 1993. Sea surface signatures related to subaqueous dunes detected by acoustic and radar sensors. Continental Shelf Research, 13: 1023-1043

29 Keller G H & A F Richards, 1967. Sediments of the Malacca Strait, Southeast Asia. Journal of Sedimentary Petrology, 37: 102-127

30 Coleman J M, 1969. Brahmaputra river: channel processes and sedimentation. Sedimentary Geology, 3: 129-239

31 Malikidis M, P T Harris & P M Tate, 1989. Sediment transport and flow over sandwaves in a non-rectilinear tidal environment: Bass Strait, Australia. Continental Shelf Research, 9: 203-221

32 Terwindt J H J, 1971. Sand waves in the southern bight of the North Sea. Marine Geology, 10: 51-67